CHEMISTRY

A mutually stabilized host-guest pair

Chi Zhang, Hongye Wang, Jie Zhong, Ye Lei, Renfeng Du, Yang Zhang, Libo Shen, Tianyu Jiao, Yulu Zhu, Haiming Zhu, Haoran Li, Hao Li*

By using click chemistry, a hexacationic cage was synthesized. The cage contains two triscationic π-electron–deficient trispyridiniumtriazine (TPZ^{3+}) platforms that are bridged in a face-to-face manner by three ethylene-triazole-ethylene linkers. A diversity of π-electron–rich guests can be recognized within the pocket of the cage, driven by host-guest π-π interactions. The cage cavity acts as a protecting group, preventing an anthracene guest from undergoing Diels-Alder reaction. Under ultraviolet (UV) light, the pyridinium C—N bonds in TPZ^{3+} platforms are polarized and weakened, resulting in the occurrence of cage decomposition via β-elimination. Guest recognition could help to prevent this UV-stimulated cage decomposition by suppressing the excitation of the TPZ^{3+} units.

INTRODUCTION

The design and syntheses of macrocyclic molecules in the form of rings (*1*, *2*), cages (*3*, *4*), capsules (*5*), and some polymeric porous materials (*6*, *7*) have always attracted great interest in the community of supramolecular chemistry. These hosts often have preorganized pockets or cavities, where various guests with complementary geometries and sizes could be accommodated and isolated from the bulk environment. As a consequence, a variety of labile molecules such as cyclobutadiene (*8*), hemiaminal (*9*, *10*), white phosphorus (*11*–*13*), benzyne (*14*), sulfur clusters (*15*), and iminiums (*16*) were able to be stabilized. Despite these many examples of the protected guest within a host, the reports of using a guest to stabilize a host are rare, except for a few self-assembled cages (*17*, *18*) containing imine linkages, which become more stable against hydrolysis in aqueous solution when the cage cavities are occupied by hydrophobic guests.

Here, we reported the synthesis of a hexacationic cage molecule via a type of click chemistry, namely, copper(I)-catalyzed alkyne-azide cycloaddition (CuAAC) (*19*). This cage bears two π-electron–deficient (TPZ^{3+}) platforms that are bridged and separated by three ethylene-triazole-ethylene linkers in a face-to-face manner by approximately 6.7 Å. The cage is able to accommodate a variety of aromatic hydrocarbons including anthracene. The anthracene guest could be protected within the cage cavity from reacting with an alkyne in bulk solution. Using a cage to encapsulate and protect a furan guest from reacting with maleimide was also reported by Smulders and Nitschke (*20*) years ago. The triazole bridges of the cage were observed to undergo ultraviolet (UV) light–stimulated β-elimination, thanks to the TPZ^{3+}, whose excited state can polarize and weaken the pyridinium C—N bonds. The UV light–stimulated β-elimination reaction could be prevented when a π-electron guest occupies the cage cavity. This is because host-guest π-π interactions efficiently quench or suppress the excitation of the TPZ^{3+} platforms in the host.

RESULTS AND DISCUSSION

Synthesis of the cage

Two precursors, namely, $\mathbf{1}^{3+}\bullet 3PF_6^-$ and $\mathbf{2}^{3+}\bullet 3PF_6^-$, which bear either three alkyne or three azide functional groups grafted on a central triscationic TPZ^{3+} moiety, were synthesized from commercially available compounds in two or three steps, respectively. These two precursors were combined in a 1:1 ratio in acetone in the presence of a $Cu(MeCN)_4PF_6$ and tris[(1-benzyl-1H-1,2,3-triazol-4-yl)methyl] amine (TBTA) ligand, which were used to catalyze CuAAC. After stirring the reaction mixture at room temperature for 12 hours, a triangular primatic cage $\mathbf{3}^{6+}\bullet 6PF_6^-$ was generated as one of the major products, which was isolated in 24% yield after performing chromatographic purification. $\mathbf{3}^{6+}\bullet 6PF_6^-$ was fully characterized by ^1H and ^{13}C nuclear magnetic resonance (NMR) spectroscopies, as well as mass spectrometry (see the Supplementary Materials).

Guest recognition ability of the cage

^1H NMR spectra recorded in CD_3CN reveal that $\mathbf{3}^{6+}$ represents a promising host to accommodate a variety of guests bearing π-electron moieties, including naphthalene, anthracene, phenanthrene, pyrene, triphenylene, perylene, and corannulene, forming a series of inclusion complexes. In the corresponding ^1H NMR spectra (Fig. 1), all of the resonances of the bound guests undergo upfield shifts, indicating that the cage cavity provides a shielded magnetic environment for the guests. By using either ^1H NMR spectroscopy or isothermal titration calorimetry (ITC), the association constants (K_a) of the corresponding inclusion complexes were determined in MeCN to be $1.9 \pm 0.2 \times 10^3$, $6.68 \pm 0.3 \times 10^4$, $81.5 \pm 7.3 \times 10^4$, $82.2 \pm 6.5 \times 10^4$, $306 \pm 30.9 \times 10^4$, $484 \pm 62.4 \times 10^4$, and $603 \pm 91.1 \times 10^4$ M^{-1} for the guests corannulene, naphthalene, anthracene, phenanthrene, pyrene, triphenylene, and perylene, respectively. In general, a guest with a larger π moiety experiences a larger K_a within the cage cavity, given that larger π moieties lead to larger π-electron interactions. This observation is consistent with the results reported by Stoddart in the **Excage**$^{6+}$ system (*21*, *22*). The remarkably smaller K_a for corannulene results from its thicker bowl-shaped geometry, which (i) leads to weaker π-π interactions and (ii) makes the corannulene less complementary to fit within the cage cavity. The occurrence of host-guest π-π interactions was convinced by UV-visible (UV-Vis) absorption spectroscopy; i.e., charge-transfer bands were observed (see fig. S15) in the UV-Vis absorption spectra of the corresponding complexes.

Diffraction grade single crystals of the inclusion complexes—including anthracene ⊂ $\mathbf{3}^{6+}$, phenanthrene ⊂ $\mathbf{3}^{6+}$, pyrene ⊂ $\mathbf{3}^{6+}$, perylene ⊂ $\mathbf{3}^{6+}$, triphenylene ⊂ $\mathbf{3}^{6+}$, and the "empty" cage $\mathbf{3}^{6+}$ (the counteranions are PF_6^-)—were obtained by vapor diffusion of isopropyl ether into the corresponding MeCN solutions of the complexes or cages, which provided (Fig. 2) unambiguous evidence for the complex formation. The distance between each of the guests and the TPZ^{3+} platforms are around 3.3 Å, confirming the occurrence of

Department of Chemistry, Zhejiang University, Hangzhou 310027, China.
*Corresponding author. Email: lihao2015@zju.edu.cn

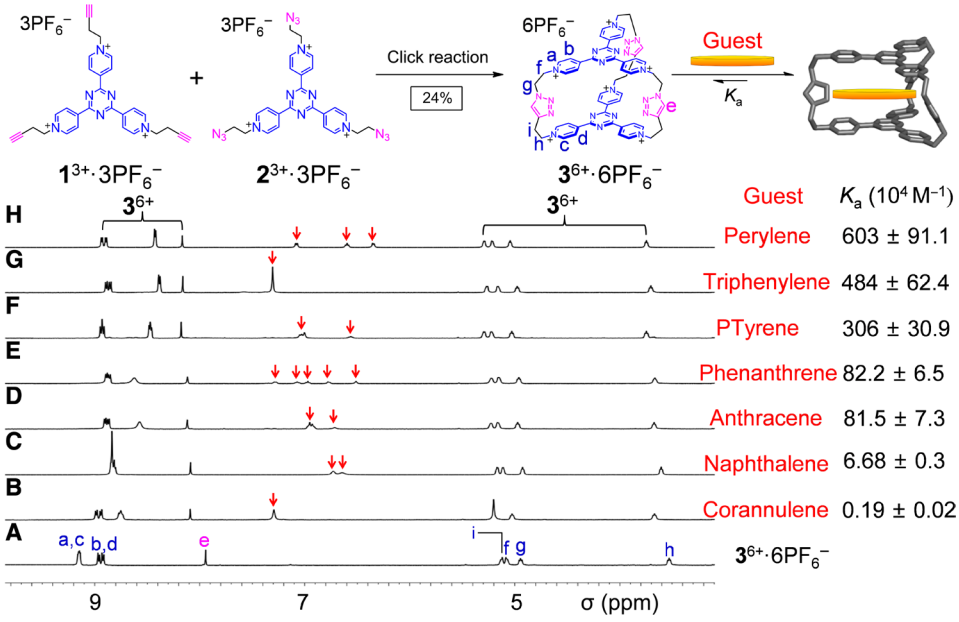

Fig. 1. Partial ^{1}H NMR spectra of the cage and its corresponding complexes after recognizing different guests. Partial ^{1}H NMR spectra (400 MHz, CD_3CN, 298 K) of the cage $\mathbf{3}^{6+}\cdot 6PF_6^-$ before (**A**) and after adding 1 eq. of one of the following guests, including (**B**) corannulene, (**C**) naphthalene, (**D**) anthracene, (**E**) phenanthrene, (**F**) pyrene, (**G**) triphenylene, and (**H**) perylene, forming the corresponding complexes. The K_a values of these complexes were listed, which were measured by either ^{1}H NMR titration for corannulene or ITC in the case of other flat guests. The resonances of the guests are labeled with red arrows.

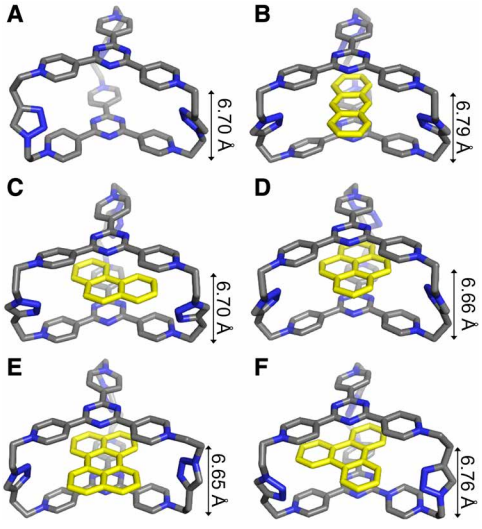

Fig. 2. Side view of the core structure of the cage and its corresponding supramolecular complexes. Side view of the core structure of (**A**) $\mathbf{3}^{6+}$, (**B**) anthracene ⊂ $\mathbf{3}^{6+}$, (**C**) phenanthrene ⊂ $\mathbf{3}^{6+}$, (**D**) pyrene ⊂ $\mathbf{3}^{6+}$, (**E**) perylene ⊂ $\mathbf{3}^{6+}$, and (**F**) triphenylene ⊂ $\mathbf{3}^{6+}$, which were obtained from single crystal x-ray diffraction experiments. Carbon, gray; nitrogen, blue; guests, yellow. The disordered solvent molecules, counteranions, and hydrogen atoms are omitted for the sake of clarity.

host-guest π-π interactions. The distances between the two TPZ^{3+} platforms of $\mathbf{3}^{6+}$ are around 6.7 Å, in the case of both "empty" cage and complexes. This consistency convinces our hypothesis that the cage has a preorganized cavity for recognizing the flat aromatic guests.

Guest protection within cage cavity

Within the cavity of $\mathbf{3}^{6+}$, the guests are isolated from the bulk environment, which prevents them from reacting with other substrates in the bulk solutions (Fig. 3A). For example, combining an electron-deficient alkyne **4** (69 mg) and anthracene (0.43 mg) in MeCN (0.6 ml) led to the formation of a Diels-Alder adduct **5**, after heating the solution at 80°C for 74 hours. The pseudo–first-order rate constant k_{obs} was determined to be 0.024 s^{-1} (Fig. 3B, black plot) by using ^{1}H NMR spectroscopy. As a comparison, after encapsulating within the cavity of the cage $\mathbf{3}^{6+}$, the rate of Diels-Alder reaction was significantly decreased. k_{obs} was measured to be 0.0029 s^{-1} (Fig. 3B, red plot), nearly one order of magnitude smaller than that in the absence of the host. Addition of a competitive guest, namely, pyrene, into the solution of anthracene ⊂ $\mathbf{3}^{6+}\cdot 6PF_6^-$ could release anthracene into the bulk solution and turn on the Diels-Alder reaction. In this condition, k_{obs} was measured to be 0.014 s^{-1} (Fig. 3B, blue plot).

Cage protection via guest accommodation

$\mathbf{3}^{6+}$ underwent decomposition via β-elimination during the irradiation of UV light (λ_{max} = 365 nm) for 8 hours (Fig. 4A), yielding $\mathbf{3a}^{5+}$ as one of the β-elimination adducts, whose formation was convinced by mass spectrometry (fig. S31). Although a similar β-elimination reaction has been reported by Chen and colleagues (*23*), during which a C—O bond was cleaved, using UV light to stimulate a β-elimination that cleaves a C—N bond without the usage of base has not been reported, to the best of our knowledge.

We reasonably hypothesize that the UV-stimulated decomposition of $\mathbf{3}^{6+}$ was initiated by activating the TPZ^{3+} platforms in the cage into an excited state. This excited state of triazine, which contains a singly occupied HOMO (highest occupied molecular orbital), is more electron-withdrawing than its ground state. As a consequence, one of the pyridinium C—N bonds becomes more polarized and therefore weakened for cleavage. This proposition was supported by the following experiments. First, we observed that a macrocycle $\mathbf{6}^{4+}\cdot 4PF_6^-$ (Fig. 4B) containing two bipyridinium moieties was relatively stable and did not undergo β-elimination upon irradiation with

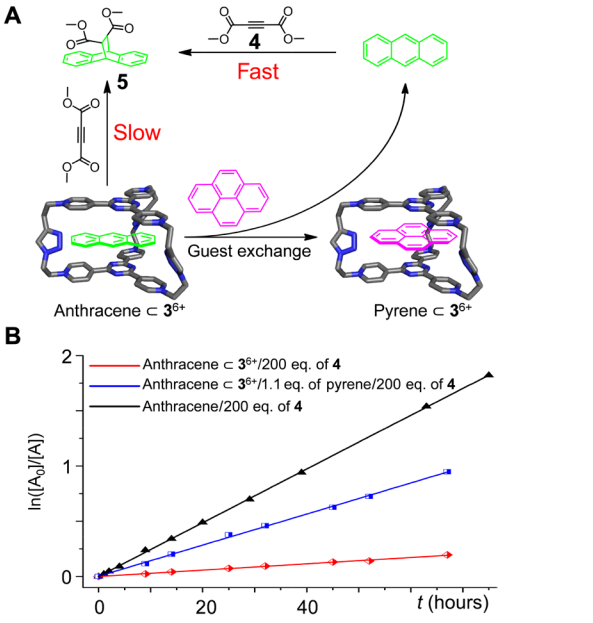

Fig. 3. Evaluation of the ability of the cage to protect an anthracene guest. (**A**) Schematic presentation of the Diels-Alder reaction between anthracene and **4** to produce **5** in the absence and presence of $\mathbf{3}^{6+}$. Within the cavity of $\mathbf{3}^{6+}$, the reaction rate of Diels reaction is much slower. When a competitive guest, namely, pyrene, drives the anthracene out from the cage cavity, the Diels-Alder reaction is turned ON. (**B**) Plots of the ln([A_0]/[A]) versus the reaction time by combining anthracene and 200 eq. of **4** in MeCN in the absence of either the cage or pyrene (black trace), in the presence of 1 eq. of $\mathbf{3}^{6+}$ (red trace), and in the presence of both 1 eq. of $\mathbf{3}^{6+}$ and 1.1 eq. of pyrene (blue trace). [A_0] and [A] represent the concentration of anthracene in the beginning and at a certain time during reaction, both of which were determined by measuring the integration of a certain proton resonance in the corresponding ^{1}H NMR spectra. The slopes of the three plots represent the apparent pseudo–first-order rate constant (k_{obs}) of the Diels-Alder reaction, which was 0.024, 0.0029, and 0.014 s^{-1}, respectively.

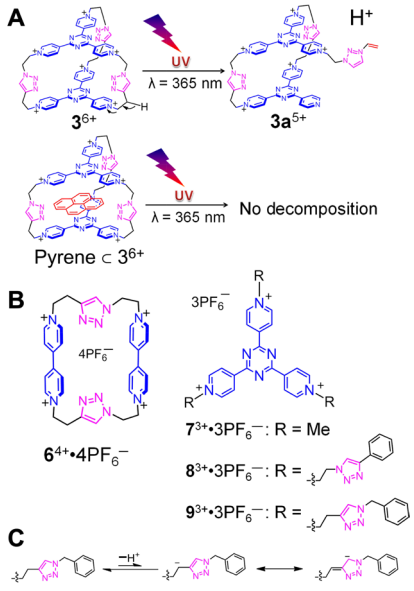

Fig. 4. UV-stimulated β-elimination of the cage and its control derivatives. (**A**) Schematic presentation of the UV-stimulated β-elimination of $\mathbf{3}^{6+}$, which produced $\mathbf{3a}^{5+}$ and a proton as one of the elimination adducts. When a pyrene guest occupies the cage cavity, β-elimination was prohibited. (**B**) Structural formulas of a tetracationic macrocycle $\mathbf{6}^{4+}$•4PF_6^- and three TPZ^{3+} derivatives $\mathbf{7}^{3+}$•3PF_6^-, $\mathbf{8}^{3+}$•3PF_6^-, and $\mathbf{9}^{3+}$•3PF_6^-. (**C**) The protons in the β-position with respect to the pyridinium nitrogen atoms in $\mathbf{9}^{3+}$•3PF_6^- are more acidic, because the negative charge of the corresponding deprotonated anion undergoes delocalization onto the triazole unit.

UV light for no less than 12 hours (see fig. S38D). This observation indicates that a triazine, which acts as a photosensitizer to polarize the C═N bonds, plays an important role in β-elimination. Second, a TPZ^{3+} derivative, namely, $\mathbf{7}^{3+}$·3PF_6^- (Fig. 4B), underwent reduction into its radical state under the protection of an atmosphere of nitrogen, namely, $\mathbf{7}^{(2+)\bullet}$, after irradiating $\mathbf{7}^{3+}$·3PF_6^- with UV light in the presence of either methanol or tetrahydrofuran (THF) as a sacrificial reagent, as inferred from the corresponding electron paramagnetic resonance (EPR) spectrum (Fig. 5B, red trace). Note that without UV light, neither methanol nor THF is capable of reducing $\mathbf{7}^{3+}$ to $\mathbf{7}^{(2+)\bullet}$. These observations indicate that TPZ^{3+} becomes more oxidative or electron-withdrawing in its excited state. This behavior is reminiscent of a few other π-electron acceptors such as naphthalene-1,8:4,5-bis(dicarboximide) (*24*) and 2,4,6-triphenylpyrylium (*25*), both of which also become more oxidative in their UV light–stimulated excited state. Last, it seems that the occurrence of β-elimination requires relatively acidic β-protons in the methylene unit with respect to the pyridinium nitrogen atom. This hypothesis is proven by the observation that upon irradiation of three TPZ^{3+} derivatives including $\mathbf{7}^{3+}$•3PF_6^-, $\mathbf{8}^{3+}$•3PF_6^-, and $\mathbf{9}^{3+}$•3PF_6^- with UV light, only $\mathbf{9}^{3+}$•3PF_6^- underwent decomposition, yielding β-elimination products $\mathbf{9a}^{2+}$ and $\mathbf{9b}^{2+}$ (see figs. S33 to S36 and S38), as well as the alkene fragment **S3** (see its molecular formula in fig. S37). The β-protons in $\mathbf{9}^{3+}$ is more acidic than those in $\mathbf{7}^{3+}$ and $\mathbf{8}^{3+}$, given that the negative charge of its deprotonated anionic form can be delocalized onto the electro-withdrawing triazole moiety (Fig. 4C). It seems that under UV light, a few other reactions besides β-elimination also occurred, which precluded our trial to calculate the yield of β-elimination of $\mathbf{3}^{6+}$. For example, under UV light, the alkene **S3** underwent oxidation, leading to the generation of an aldehyde **S4** (see its molecular formula in fig. S37).

When the cavity of $\mathbf{3}^{6+}$ was occupied by a guest such as anthracene, phenanthrene, pyrene, and triphenylene, the UV light–stimulated cage decomposition was avoided; i.e., no appreciable decomposition was observed (figs. S39 and S40) after irradiating the complex for no less than 12 hours. This is because the guest molecule introduces π-π interactions, which could prevent or suppress the UV-stimulated excitation of TPZ^{3+} units. This proposition is supported by the following experiments.

First, cyclic voltammograms of $\mathbf{3}^{6+}$•6PF_6^- (Fig. 5A, black trace) and pyrene ⊂ $\mathbf{3}^{6+}$•6PF_6^- (Fig. 5A, red trace) were recorded in MeCN. One of the two TPZ^{3+} units in the complex pyrene ⊂ $\mathbf{3}^{6+}$•6PF_6^- has a more negative reduction potential, i.e., −730 mV, compared to −635 mV in the case of empty cage. The implication is that the LUMO (lowest unoccupied molecular orbital) of TPZ^{3+} is increased by 0.095 eV and that the compound becomes more difficult to reduce when it undergoes π-π interactions with a pyrene guest. The increase of LUMO of the TPZ^{3+} thus results in the failure or difficulty of generating the excited state, as a consequence of which, β-elimination did not occur. Second, high-energy excited state decay kinetics for $\mathbf{3}^{6+}$•6PF_6^- in the absence and presence of a pyrene guest at UV light excitation (365 nm) were probed by transient absorption spectra (Fig. 5C and fig. S42). It is obvious that the excited

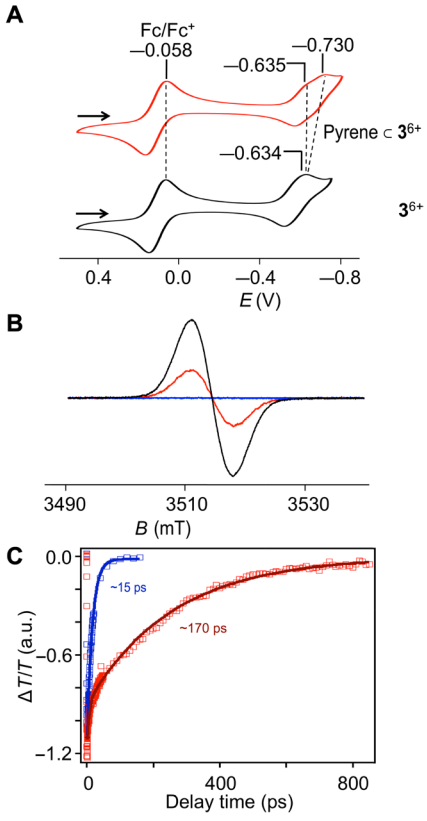

Fig. 5. Mechanism investigation of the cage protection via guest accommodation. (**A**) Second scans of the cyclic voltammograms (CVs) for $\mathbf{3}^{6+}\bullet 6PF_6^-$ (black trace) and pyrene ⊂ $\mathbf{3}^{6+}\bullet 6PF_6$ (red trace). The reduction peak observed at −0.058 V corresponds to the reduction process of a reference compound, namely, ferrocene/ferrocene$^+$ (Fc/Fc^+). All the CVs were recorded under the same conditions of temperature (298 K), solvent (argon-purged MeCN), concentrations (1 mM), and tetrabutylammonium hexafluorophosphate electrolyte (0.1 M). The scan rate was set at 200 mV s^{-1}. (**B**) EPR spectra of $\mathbf{7}^{3+}\bullet 3PF_6^-$ under the irradiation of UV light at 365 nm in the presence of THF as a sacrificial reductant in the absence (red trace) and in the presence of 8 eq. of pyrene (blue trace). The EPR signal of the red trace indicates the formation of $\mathbf{7}^{(2+)\bullet}$ radical. The black trace corresponds to a solution of $\mathbf{7}^{(2+)\bullet}$, which was produced by adding Zn dust as a reductant into a MeCN solution of $\mathbf{7}^{3+}\bullet 3PF_6^-$. (**C**) Time-resolved absorption spectra of $\mathbf{3}^{6+}\bullet 6PF_6^-$ (red trace) and pyrene ⊂ $\mathbf{3}^{6+}\bullet 6PF_6$ (blue trace) upon stimulation by UV light at 365 nm. a.u., arbitrary units.

state of the TPZ^{3+} units in the complex pyrene ⊂ $\mathbf{3}^{6+}\bullet 6PF_6^-$ (Fig. 5C, blue trace) decays much faster to ground state (~15 ps) compared to those of the cage $\mathbf{3}^{6+}\bullet 6PF_6^-$ itself (~ 170 ps) (Fig. 5C, red trace), likely suppressing the deposition process in the former. Third, π-π interactions were observed to prevent the UV light–stimulated reduction of $\mathbf{7}^{3+}$; i.e., irradiation of $\mathbf{7}^{3+}$ with UV light (λ_{max} = 365 nm) in the presence of 8 eq. of pyrene and a sacrificial reductant did not produce the radical $\mathbf{7}^{(2+)\bullet}$, as inferred from the corresponding silent EPR spectrum (Fig. 5B, blue trace). These experiments all help to convince that host protection was accomplished by means of host-guest π-electron donor-acceptor interactions that suppress the UV light–stimulated excitation of TPZ^{3+}.

CONCLUSION

In summary, we synthesized a hexacationic cage by means of click reaction. This cage has a preorganized cavity for recognizing a variety of aromatic guests, including anthracene and pyrene. On one hand, the cage acts as a molecular container, which isolates anthracene from bulk environment and therefore protects it from undergoing Diels-Alder reaction. On the other hand, the triazole bridges in the cage undergo β-elimination under UV light irradiation, during which the TPZ^{3+} units in the cage could be activated into their excited state and promote the cleavage of C—N bonds. Because a guest such as pyrene could introduce π-π donor-acceptor interactions that quenched or suppressed the UV light–stimulated excited state of TPZ^{3+}, host protection could thus be achieved by guest recognition. The use of small molecular components to block the reaction pathway of a large system and influence its properties will likewise be developed.

MATERIALS AND METHODS

All reagents and solvents were purchased from commercial sources and used without further purification. Solvents were deoxygenated by passing N_2 through the solvent for 30 min. Manipulations were performed under a normal laboratory atmosphere unless otherwise noted. $\mathbf{7}^{3+}\bullet 3PF_6^{-S1}$, $\mathbf{S1}^{2+}\bullet 2PF_6^{-S2}$, and $\mathbf{S2}^{2+}\bullet 2PF_6^{-S3}$ were synthesized as previously reported. NMR spectra were recorded at ambient temperature using Bruker AVANCE III 400/500 or Agilent DD2 600 spectrometers, with working frequencies of 400, 500, and 600 MHz and 100, 125, and 150 MHz for ^1H and ^{13}C, respectively. Chemical shifts are reported in parts per million (ppm) relative to the residual internal nondeuterated solvent signals (CD_3CN, δ = 1.94 ppm; $CDCl_3$, δ = 7.27 ppm). High-resolution mass spectra (HRMS) were measured using a Shimadzu liquid chromatography–mass spectrometry ion trap time-of-flight instrument. X-ray crystallographic data were collected on a Bruker D8 Venture diffractometer. ITC experiments were performed on a MicroCal system, VP-ITC model. EPR spectra were taken on a continuous-wave EPR spectrometer (Bruker A300), and the samples were injected into a glass capillary and put into the cavity. The EPR spectra were recorded in X-band at room temperature with a microwave power of 0.2 mW, a modulation frequency of 100 kHz, and a modulation amplitude of 1 G. The *g* factors were corrected with respect to that of an equipped *g* marker (1,1-diphenyl-2-picrylhydrazyl, *g* = 2.0036). UV-Vis-NIR absorption spectra were taken on a Cary Series UV-Vis-NIR spectrophotometer.

SUPPLEMENTARY MATERIALS

Supplementary material for this article is available at http://advances.sciencemag.org/cgi/content/full/5/11/eaax6707/DC1

Scheme S1. Synthesis of $\mathbf{1}^{3+}\cdot 3PF_6^-$.
Scheme S2. Synthesis of $\mathbf{2}^{3+}\cdot 3PF_6^-$.
Scheme S3. Synthesis of $\mathbf{3}^{6+}\cdot 6PF_6^-$.
Scheme S4. Synthesis of $\mathbf{6}^{4+}\cdot 4PF_6^-$.
Scheme S5. Synthesis of $\mathbf{8}^{3+}\cdot 3PF_6^-$.
Scheme S6. Synthesis of $\mathbf{9}^{3+}\cdot 3PF_6^-$.
Fig. S1. ^1H and ^{13}C spectrum of $\mathbf{3}^{6+}\cdot 6PF_6^-$.
Fig. S2. ^1H-^1H correlation spectroscopy (500 MHz, D_2O, 298 K) spectrum of $\mathbf{3}^{6+}\cdot 6PF_6^-$.
Fig. S3. Electrospray ionization–HRMS of $\mathbf{3}^{6+}\cdot 6PF_6^-$.
Fig. S4. ^1H and ^{13}C spectrum of $\mathbf{6}^{4+}\cdot 4PF_6^-$.
Fig. S5. ^1H-^1H correlation spectroscopy spectrum (500 MHz, D_2O, 298 K) of $\mathbf{6}^{4+}\cdot 4PF_6^-$.
Fig. S6. Electrospray ionization–HRMS of $\mathbf{6}^{4+}\cdot 4PF_6^-$.
Fig. S7. ^1H NMR spectrum (400 MHz, CD_3CN, 298 K) of $\mathbf{3}^{6+}\cdot 6PF_6^-$ (1.34 mM) upon addition of different amount of anthracene.
Fig. S8. ^1H NMR spectrum (400 MHz, CD_3CN, 298 K) of $\mathbf{3}^{6+}\cdot 6PF_6^-$ (1.34 mM) upon addition of different amount of phenanthrene.
Fig. S9. ^1H NMR spectrum (400 MHz, CD_3CN, 298 K) of $\mathbf{3}^{6+}\cdot 6PF_6^-$ (1.34 mM) upon addition of different amount of pyrene.

Fig. S10. ^{1}H NMR spectrum (400 MHz, CD_3CN, 298 K) of $\mathbf{3}^{6+}\cdot 6PF_6^-$ (1.34 mM) upon addition of different amount of triphenylene.
Fig. S11. ^{1}H NMR spectrum (400 MHz, CD_3CN, 298 K) of $\mathbf{3}^{6+}\cdot 6PF_6^-$ (1.34 mM) upon addition of different amount of corannulene.
Fig. S12. ^{1}H NMR spectrum (400 MHz, CD_3CN, 298 K) of the mixture of $\mathbf{7}^{6+}\cdot 3PF_6^-$ (1.34 mM) and 6eqiv of corannulene and $\mathbf{7}^{6+}\cdot 3PF_6^-$ (1.34 mM).
Fig. S13. Plot of the upfield shifts of the resonance of proton e (assigned in fig. S11) of $\mathbf{3}^{6+}\cdot 6PF_6^-$.
Fig. S14. UV-Vis absorption spectrum of $\mathbf{3}^{6+}\cdot 6PF_6^-$ at 0.5 μM in MeCN at 298 K.
Fig. S15. UV-Vis absorption spectra of polycyclic aromatic hydrocarbon (PAH) guests, $\mathbf{3}^{6+}\cdot 6PF_6^-$, and the corresponding 1:1 complexes in MeCN at 298 K.
Fig. S16. Fluorescence spectra of the $\mathbf{3}^{6+}\cdot 6PF_6^-$ (1×10^{-3} mM) after addition of different equivalents of PAH guests.
Fig. S17. Titration plots (heat rate versus time and heat versus guest/host ratio) obtained from ITC experiments of $\mathbf{3}^{6+}\cdot 6PF_6^-$ (0.1 mM, 1.4 ml) with naphthalene (2 mM, 0.4 ml) in CH_3CN (298 K).
Fig. S18. Titration plots (heat rate versus time and heat versus guest/host ratio) obtained from ITC experiments of $\mathbf{3}^{6+}\cdot 6PF_6^-$ (0.1 mM, 1.4 ml) with anthracene (2 mM, 0.4 ml) in CH_3CN (298 K).
Fig. S19. Titration plots (heat rate versus time and heat versus guest/host ratio) obtained from ITC experiments of $\mathbf{3}^{6+}\cdot 6PF_6^-$ (0.1 mM, 1.4 ml) with phenanthrene (2 mM, 0.4 ml) in CH_3CN (298 K).
Fig. S20. Titration plots (heat rate versus time and heat versus guest/host ratio) obtained from ITC experiments of $\mathbf{3}^{6+}\cdot 6PF_6^-$ (0.1 mM, 1.4 ml) with pyrene (2 mM, 0.4 ml) in CH_3CN (298 K).
Fig. S21. Titration plots (heat rate versus time and heat versus guest/host ratio) obtained from ITC experiments of $\mathbf{3}^{6+}\cdot 6PF_6^-$ (0.1 mM, 1.4 ml) with triphenylene (2 mM, 0.4 ml) in CH_3CN (298 K).
Fig. S22. Titration plots (heat rate versus time and heat versus guest/host ratio) obtained from ITC experiments of $\mathbf{3}^{6+}\cdot 6PF_6^-$ (0.1 mM, 1.4 ml) with perylene (2 mM, 0.4 ml) in CH_3CN (298 K).
Fig. S23. Titration plots (heat rate versus time and heat versus guest/host ratio) obtained from ITC experiments of $\mathbf{3}^{6+}\cdot 6PF_6^-$ (0.1 mM, 1.4 ml) with corannulene (2 mM, 0.4 ml) in CH_3CN (298 K).
Fig. S24. ^{1}H NMR spectra (500 MHz, CD_3CN, 298 K) of a 1:100 mixture of anthracene and **4** recorded by heating the mixture at 343 K for a certain amount of time.
Fig. S25. ^{1}H NMR spectra (500 MHz, CD_3CN, 298 K) of a 1:150 mixture of anthracene and **4** recorded by heating the mixture at 343 K for a certain amount of time.
Fig. S26. ^{1}H NMR spectra (500 MHz, CD_3CN, 298 K) of a 1:200 mixture of anthracene and **4** recorded by heating the mixture at 343 K for a certain amount of time.
Fig. S27. ^{1}H NMR spectra (500 MHz, CD_3CN, 298 K) of a 1:1:200 mixture of anthracene, $\mathbf{3}^{6+}\cdot 6PF_6^-$, and **4**, which were recorded by heating the mixture at 343 K for a specific amount of time.
Fig. S28. ^{1}H NMR spectra (500 MHz, CD_3CN, 298 K) of a 1:1:1.1:200 mixture of anthracene, $\mathbf{3}^{6+}\cdot 6PF_6^-$, pyrene, and **4**, which were recorded by heating the mixture at 343 K for a specific amount of time.
Fig. S29. Plots of $-\ln([A]/[A_0])$ versus reaction time of the Diel-Alder reactions of anthracene and the alkyne **4** in different reaction conditions.
Fig. S30. ^{1}H NMR spectra (500 MHz, CD_3CN, 298 K) of $\mathbf{3}^{6+}\cdot 6PF_6^-$ after irradiating the sample with UV light (λ_{max} = 365 nm) for a special amount of time.
Fig. S31. ESI-HRMS of a solution of $\mathbf{3}^{6+}\cdot 6PF_6^-$ in MeCN, upon irradiation with UV light (λ_{max} = 365 nm) for 8 hours.
Fig. S32. ESI-MS of a solution of $\mathbf{3}^{6+}\cdot 6PF_6^-$ in MeCN, upon irradiation with UV light (λ_{max} = 365 nm) for a special amount of time.
Fig. S33. ^{1}H NMR spectra (500 MHz, CD_3CN, 298 K) of $\mathbf{9}^{3+}\cdot 3PF_6^-$ after irradiating the sample with UV light (λ_{max} = 365 nm) for a special amount of time.
Fig. S34. ESI-HRMS of a solution of $\mathbf{9}^{3+}\cdot 3PF_6^-$ in MeCN, upon irradiation with UV light (λ_{max} = 365 nm) for 8 hours.
Fig. S35. ESI-MS of a solution of $\mathbf{9}^{3+}\cdot 3PF_6^-$ in MeCN, upon irradiation with UV light (λ_{max} = 365 nm) for a special amount of time.
Fig. S36. ^{1}H NMR spectrum (500 MHz, CD_3CN, 298 K) of $\mathbf{9a}^{2+}\cdot 2PF_6^-$, which was obtained from the UV light irradiation reaction mixture (used for fig. S33) by means of chromatographic purification.
Fig. S37. ^{1}H NMR spectra (500 MHz, CD_3CN, 298 K) of the solution containing **S3** and **S4**.
Fig. S38. Partial ^{1}H NMR spectra (400 MHz, CD_3CN, 298 K) of $\mathbf{7}^{3+}\cdot 3PF_6^-$, $\mathbf{6}^{4+}\cdot 4PF_6^-$, and $\mathbf{8}^{3+}\cdot 3PF_6^-$, before and after UV light irradiation (λ_{max} = 356 nm).
Fig. S39. ^{1}H NMR spectra (500 MHz, CD_3CN, 298 K) of a complex pyrene ⊂ $\mathbf{3}^{6+}\cdot 6PF_6^-$ after the sample was irradiated under UV light (λ_{max} = 365 nm) for a special amount of time.
Fig. S40. Partial ^{1}H NMR spectra (400 MHz, CD_3CN, 298 K) of $\mathbf{3}^{6+}\cdot 6PF_6^-$ under UV light (λ_{max} = 365 nm) in the presence of 1.1 eq. of PAH guests.
Fig. S41. Partial ^{1}H NMR spectra of $\mathbf{9}^{3+}\cdot 3PF_6^-$ under UV light (λ_{max} = 365 nm) for 12 hours in the presence of different equivalents of pyrene.
Fig. S42. Transient absorption spectra of $\mathbf{3}^{6+}\cdot 6PF_6^-$ and pyrene ⊂ $\mathbf{3}^{6+}\cdot 6PF_6^-$ under UV light excitation.
Fig. S43. Different views of the solid-state structure of $\mathbf{3}^{6+}\cdot 6PF_6^-$.
Fig. S44. Different views of the solid-state structure of anthracene ⊂ $\mathbf{3}^{6+}\cdot 6PF_6^-$.
Fig. S45. Different views of the solid-state structure of phenanthrene ⊂ $\mathbf{3}^{6+}\cdot 6PF_6^-$.
Fig. S46. Different views of the solid-state structure of pyrene ⊂ $\mathbf{3}^{6+}\cdot 6PF_6^-$.
Fig. S47. Different views of the solid-state structure of triphenylene ⊂ $\mathbf{3}^{6+}\cdot 6PF_6^-$.
Fig. S48. Different views of the solid-state structure of perylene ⊂ $\mathbf{3}^{6+}\cdot 6PF_6^-$.
Table S1. K_a values and thermodynamic parameters for the 1:1 complexes formed between $\mathbf{3}^{6+}\cdot 6PF_6^-$ and PAH guests in MeCN at 25°C.
References (*26*–*31*)

REFERENCES AND NOTES

1. C. J. Pedersen, Cyclic polyethers and their complexes with metal salts. *J. Am. Chem. Soc.* **89**, 7017–7036 (1967).
2. C. J. Pedersen, Cyclic polyethers and their complexes with metal salts. *J. Am. Chem. Soc.* **89**, 2495–2496 (1967).
3. M. Fujita, D. Oguro, M. Miyazawa, H. Oka, K. Yamaguchi, K. Ogura, Self-assembly of ten molecules into nanometre-sized organic host frameworks. *Nature* **378**, 469–471 (1995).
4. D. J. Cram, Cavitands: Organic hosts with enforced cavities. *Science* **219**, 1177–1183 (1983).
5. T. Heinz, D. M. Rudkevich, J. Rebek Jr., Pairwise selection of guests in a cylindrical molecular capsule of nanometre dimensions. *Nature* **394**, 764–766 (1998).
6. J. Tian, Z.-Y. Xu, D.-W. Zhang, H. Wang, S.-H. Xie, D.-W. Xu, Y.-H. Ren, H. Wang, Y. Liu, Z.-T. Li, Supramolecular metal-organic frameworks that display high homogeneous and heterogeneous photocatalytic activity for H_2 production. *Nat. Commun.* **7**, 11580 (2016).
7. J. Tian, T.-Y. Zhou, S.-C. Zhang, S. Aloni, M. V. Altoe, S.-H. Xie, H. Wang, D. W. Zhang, X. Zhao, Y. Liu, Z.-T. Li, Three-dimensional periodic supramolecular organic framework ion sponge in water and microcrystals. *Nat. Commun.* **5**, 5574 (2014).
8. D. J. Cram, M. E. Tanner, R. Thomas, The taming of cyclobutadiene. *Angew. Chem. Int. Ed.* **30**, 1024–1027 (1991).
9. T. Iwasawa, R. J. Hooley, J. Rebek Jr., Stabilization of labile carbonyl addition intermediates by a synthetic receptor. *Science* **317**, 493–496 (2007).
10. R. J. Hooley, T. Iwasawa, J. Rebek, Detection of reactive tetrahedral intermediates in a deep cavitand with an introverted functionality. *J. Am. Chem. Soc.* **129**, 15330–15339 (2007).
11. P. Mal, B. Breiner, K. Rissanen, J. R. Nitschke, White phosphorus is air-stable within a self-assembled tetrahedral capsule. *Science* **324**, 1697–1699 (2009).
12. D. Yang, J. Zhao, L. Yu, X.-S. Lin, W.-Y. Zhang, H.-W. Ma, A. Gogoll, Z.-B. Zhang, Y.-Y. Wang, X.-J. Yang, B. Wu, Air- and light-stable P_4 and As_4 within an anion-coordination-based tetrahedral cage. *J. Am. Chem. Soc.* **139**, 5946–5951 (2017).
13. T.-Y. Jiao, L. Chen, D. Yang, X. Li, G.-C. Wu, P.-M. Zeng, A.-K. Zhou, Q. Yin, Y.-J. Pan, B. Wu, X. Hong, X.-Q. Kong, V. M. Lynch, J. L. Sessler, H. Li, Trapping white phosphorus within a purely organic molecular container produced by imine condensation. *Angew. Chem. Int. Ed.* **56**, 14545–14550 (2017).
14. R. Warmuth, *o*-Benzyne: Strained alkyne or cumulene?—NMR characterization in a molecular container. *Angew. Chem. Int. Ed.* **36**, 1347–1350 (1997).
15. S. Matsuno, M. Yamashina, Y. Sei, M. Akita, A. Kuzume, K. Yamamoto, M. Yoshizawa, Exact mass analysis of sulfur clusters upon encapsulation by a polyaromatic capsular matrix. *Nat. Commun.* **8**, 749 (2017).
16. V. M. Dong, D. Fiedler, B. Carl, R. G. Bergman, K. N. Raymond, Molecular recognition and stabilization of iminium ions in water. *J. Am. Chem. Soc.* **128**, 14464–14465 (2006).
17. C. Givelet, J.-L. Sun, D. Xu, T. J. Emge, A. Dhokte, R. Warmuth, Templated dynamic cryptophane formation in water. *Chem. Commun.* **47**, 4511–4513 (2011).
18. Z.-H. Lin, J.-L. Sun, B. Efremovska, R. Warmuth, Assembly of water-soluble, dynamic, covalent container molecules and their application in the room-temperature stabilization of protoadamantene. *Chem. A Eur. J.* **18**, 12864–12872 (2012).
19. R. Huisgen, G. Szeimies, L. Möbius, 1.3-Dipolare Cycloadditionen, XXXII. Kinetik der Additionen Organischer Azide an CC-Mehrfachbindungen. *Chem. Ber.* **100**, 2494–2507 (1967).
20. M. M. J. Smulders, J. R. Nitschke, Supramolecular control over Diels–Alder reactivity by encapsulation and competitive displacement. *Chem. Sci.* **3**, 785–788 (2012).
21. E. J. Dale, N. A. Vermeulen, A. A. Thomas, J. C. Barnes, M. Juríček, A. K. Blackburn, N. L. Strutt, A. A. Sarjeant, C. L. Stern, S. E. Denmark, J. F. Stoddart, ExCage. *J. Am. Chem. Soc.* **136**, 10669–10682 (2014).
22. N. Hafezi, J. M. Holcroft, K. J. Hartlieb, E. J. Dale, N. A. Vermeulen, C. L. Stern, A. A. Sarjeant, J. F. Stoddart, Modulating the binding of polycyclic aromatic hydrocarbons inside a hexacationic cage by anion–π interactions. *Angew. Chem. Int. Ed.* **54**, 456–461 (2015).
23. Z. Meng, J.-F. Xiang, C.-F. Chen, Directional molecular transportation based on a catalytic stopper-leaving rotaxane system. *J. Am. Chem. Soc.* **138**, 5652–5658 (2016).
24. Q. Song, F. Li, Z.-Q. Wang, X. Zhang, A supramolecular strategy for tuning the energy level of naphthalenediimide: promoted formation of radical anions with extraordinary stability. *Chem. Sci.* **6**, 3342–3346 (2015).
25. M. A. Miranda, H. Garcia, 2,4,6-Triphenylpyrylium tetrafluoroborate as an electron-transfer photosensitizer. *Chem. Rev.* **94**, 1063–1089 (1994).
26. V. D. Nguyen, C. A. McCormick, F. A. Vaccaro, K. E. Riley, C. J. Stephenson, J. T. Mague, L. V. Koplitz, Two red salts derived from yellow 4-cyano-1-methylpyridinium iodide: 1,1′,1″-trimethyl-4,4′,4″-(1,3,5-triazin-2,4,6-triyl)tripyridinium trisiodide and 4-cyano-1-methylpyridinium triiodide. *Polyhedron* **114**, 428–434 (2016).
27. H. R. Wessels, C. Slebodnick, H. W. Gibson, Viologen-based rotaxanes from dibenzo-30-crown-10. *J. Am. Chem. Soc.* **140**, 7358–7370 (2018).
28. A. Coskun, S. Saha, I. Aprahamian, J. F. Stoddart, A reverse donor-acceptor bistable [2] catenane. *Org. Lett.* **10**, 3187–3190 (2008).

29. O. V. Dolomanov, L. J. Bourhis, R. J. Gildea, J. A. K. Howard, H. Puschmann, OLEX2: A complete structure solution, refinement and analysis program. *J. Appl. Cryst.* **42**, 339–341 (2009).
30. G. M. Sheldrick, SHELXT—Integrated space-group and crystal-structure determination. *Acta Crystallogr.* **71**, 3–8 (2015).
31. G. M. Sheldrick, Crystal structure refinement with *SHELXL*. *Acta Crystallogr.* **C71**, 3–8 (2015).

Acknowledgments
Funding: This work was supported by the National Natural Science Foundation of China (nos. 91856116 and 21772173), the Natural Science Foundation of Zhejiang Province (no. LR18B020001), and "the Fundamental Research Funds for the Central Universities" (no. 2019FZA3007). **Author contributions:** C.Z. and Hao Li designed experiments. C.Z., H.W., J.Z., Y.L., R.D., Y. Zhang, L.S., T.J., and Y. Zhu performed experiments. C.Z. and Hao Li wrote the manuscript. H.Z., Haoran Li, and Hao Li edited the manuscript. **Competing interests:** The authors declare that they have no competing interests. **Data and materials availability:** All data needed to evaluate the conclusions in the paper are present in the paper and/or the Supplementary Materials. Additional data related to this paper may be requested from the authors.

Submitted 11 April 2019
Accepted 16 September 2019
Published 1 November 2019
10.1126/sciadv.aax6707

Citation: C. Zhang, H. Wang, J. Zhong, Y. Lei, R. Du, Y. Zhang, L. Shen, T. Jiao, Y. Zhu, H. Zhu, H. Li, H. Li, A mutually stabilized host-guest pair. *Sci. Adv.* **5**, eaax6707 (2019).